

## SUPPORTING CREWED LUNAR EXPLORATION WITH LIAISON NAVIGATION

Jason M. Leonard,<sup>\*</sup> Jeffrey S. Parker,<sup>†</sup> Rodney L. Anderson,<sup>‡</sup>  
Ryan M. McGranaghan,<sup>\*</sup> Kohei Fujimoto,<sup>\*</sup> and George H. Born<sup>§</sup>

This paper examines the benefits of navigating a crewed vehicle between the Earth and the Moon using both ground tracking and satellite-to-satellite tracking. Linked Autonomous Interplanetary Satellite Orbit Navigation (LiAISON) is a new technique that has been shown to dramatically improve the navigation of lunar satellites, libration orbiters, and Earth orbiting satellites using scalar inter-satellite observations. In this paper, LiAISON is applied to the problem of navigating a crewed vehicle to the Moon. It has been found that LiAISON observations improve the navigation accuracy enough to reduce the number of active ground tracking stations from six to three.

### INTRODUCTION

Historically, crewed vehicles behave significantly different than that of a robotic spacecraft. While a robotic spacecraft is considered to be a quiet vehicle (performing maneuvers infrequently, passive thermal controls, minimal venting, etc.), crewed vehicles typically experience significant statistical accelerations that have unknown or poorly modeled characteristics. During the Apollo era, it was determined that significant deviations in the trajectory occurred due to the activity of the crew and certain outgassing or maneuver events.<sup>1,2</sup>

The Apollo lunar missions required an extensive number of ground stations in order to obtain a reasonable state uncertainty. While the Deep Space Network (DSN) has been significantly advanced since the Apollo era and future spacecraft will be quieter in terms of unmodeled accelerations, three tracking stations alone are not sufficient to accurately estimate future crewed missions.<sup>3,4</sup> One possible solution that has been put forth is that of introducing additional tracking stations culminating in the IDAC4B configuration.<sup>5</sup> The proposed IDAC4B configuration utilizes the three DSN stations and three other tracking stations located in the opposite hemisphere. While this configuration is enough to obtain uncertainties necessary for a crewed mission to the Moon, infrastructure costs are significantly increased due to the additional stations.

LiAISON is motivated by NASA's aim to develop a permanent presence at the Moon while supplementing current tracking networks to obtain similar or better navigation accuracies. The

---

<sup>\*</sup> Research Assistant, Colorado Center for Astrodynamics Research, University of Colorado, Boulder, CO 80309.

<sup>†</sup> Assistant Research Professor at the University of Colorado, Boulder, CO 80309.

<sup>‡</sup> Member of Technical Staff, Jet Propulsion Laboratory, California Institute of Technology, M/S 301-121, 4800 Oak Grove Dr., Pasadena, CA 91109.

<sup>§</sup> Professor at the University of Colorado, Boulder, CO 80309.

LiAISON concept consists of collecting simple radiometric tracking signals between two or more satellites, and using those signals to supplement or replace ground-based tracking and navigation. Several architecture concepts are possible from cooperative LiAISON constellations to a single LiAISON based navigation beacon that provides a GPS-like capability for lunar missions as well as Earth orbiting satellites. LiAISON alleviates the heavy dependence on current ground-based time and state vector updates, allowing spacecraft to do autonomous navigation updates on-board with only satellite-to-satellite radiometric data.

Hill et al. explored the use of multiple satellites placed in combinations of low lunar orbits and libration orbits about the Earth-Moon Libration points EML-1 and/or EML-2.<sup>6-9</sup> A potential mission was examined, including only two satellites: one in a 100-km polar orbit about the Moon and the other in an libration point orbit (LPO) about the EML-2 point.<sup>7</sup> The results demonstrated that satellites may be navigated at the Moon using realistic constraints and achieve uncertainties on the order of 100 meters root sum squared (RSS) or less for halo orbiters and 10 meters or less RSS for low lunar orbiters. Any ground tracking passes would only improve the solutions.

A LiAISON constellation configuration involving two satellites, one in a halo orbit about EML-1 and one in geosynchronous Earth orbit, has also been analyzed previously. References 10 and 11 demonstrated that the relative and absolute navigation of two satellites at GEO and EML-1 is possible through the use of satellite-to-satellite range and range-rate measurements. In addition, this measurement type can supplement and significantly improve radiometric measurements taken from the DSN for satellite navigation.

This study examines various navigation architectures, including ground-based and LiAISON-supplemented configurations, for a crewed mission to the Moon. A crewed trans-lunar cruise mission is designed with a navigation satellite located at EML-1. Both ground-based tracking and LiAISON tracking support the crewed mission. An acceleration uncertainty model is developed based on Apollo era uncertainties to reflect a noisy crewed vehicle. Several tracking architectures are then compared. Finally, the sensitivity of navigation uncertainty due to the strength of the acceleration uncertainty is determined.

## **LIAISON NAVIGATION**

Autonomous satellite-to-satellite tracking relies on an ability to estimate the absolute positions of a spacecraft without the use of ground station observations. To do so, the size, shape, and orientation of the satellite's orbit must be observable from the measurements available between the linked spacecraft. The observability of the system depends on one of these satellites occupying a unique trajectory. The determining factor in whether a unique trajectory can exist, and thus whether LiAISON is possible, is the acceleration function acting on the orbiter. No unique orbits exist in a symmetric acceleration field, such as a simple Earth two-body model.

The success of LiAISON navigation is enabled by the ability to model the acceleration field with sufficient accuracy to identify the unique path of the spacecraft through that field. Acceleration functions with sufficient asymmetry for LiAISON are provided by three-body systems that give rise to LPOs. The lunar libration point force field including perturbations from other planets and solar radiation is modeled to sufficient accuracy to make autonomous navigation possible. EML-1 and EML-2 LPOs are specifically well suited for LiAISON because they are locally unique and reside in regions where the asymmetry of the accelerations is strong. Under these conditions, a spacecraft at one of these Lagrange points can uniquely and absolutely determine the state of a second satellite using crosslink measurements without ground-based observations. Unlike GPS and similar satellite-to-satellite tracking systems, LiAISON does not require any a priori knowledge of either spacecraft's state.

## MISSION DESIGN

The reference mission designed for this study involves two spacecraft: one is a navigation satellite in a halo orbit about EML-1 and the other is a crewed spacecraft on a trans-lunar cruise (TLC). Figure 1 illustrates the tracking network used in this study that helps support a crewed spacecraft traveling from the Earth to the Moon that includes ground observations from the DSN as well as SST measurements obtained from a LiAISON navigation satellite near EML-1.

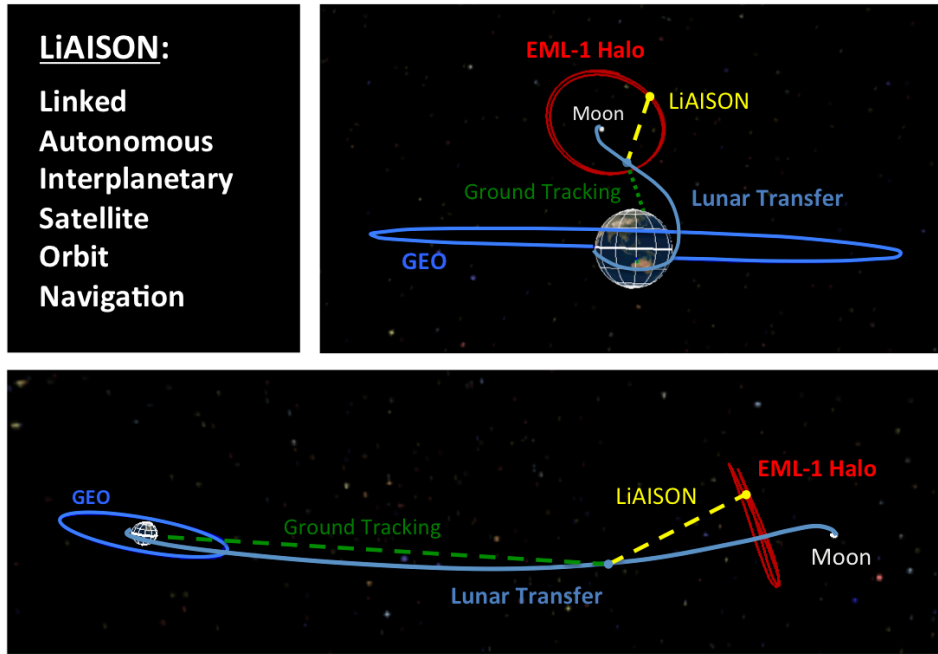


**Figure 1. LiAISON constellation for an EML-1 navigation satellite and a crewed spacecraft on TLC. The plots are visualized in the Earth-Moon rotating frame.**

There are several potential benefits of this LiAISON configuration. First, the EML-1 navigation satellite would have near-continuous communication with the spacecraft in TLC. The variation in geometry of the EML-1 navigation satellite and the TLC spacecraft provides significant information for tracking when compared to ground tracking. This variation in geometry allows for more information in the radial, in-track, and cross-track directions when compared to conventional DSN radiometric data.

### **Lunar $L_1$ Halo Orbit**

This work assumes that there is already a dedicated navigation satellite in a halo orbit located at EML-1. The orbit is similar to that of the ARTEMIS mission that traversed the EML-1 point in 2010 and 2011.<sup>12,13</sup> The halo reference orbit used in this study was generated using a two-step process. First, the analytical expansion described by Richardson and Cary was used to generate a set of initial states.<sup>14</sup> The reference epoch for the initial state is defined as January 1, 2020 ET (Ephemeris Time). The amplitude of the z-axis for the halo orbiter,  $A_z$ , has been set to 35,500 km. The initial phase angle of the orbit,  $\phi$ , has been set to zero degrees. The parameters used to generate the reference trajectory are given in Table 1.

**Table 1. EML-1 quasi-halo orbit parameters.**

Parameter	Value	Comments
$A_z$	35,500 km	The z-axis amplitude
$\phi$	0 deg	The initial phase angle of the orbit
$t_{ref}$	1/1/2020 00:00:00 ET	The reference epoch, ephemeris time

A set of six revolutions with four states per revolution of the halo orbit is used to describe the desired reference trajectory. Reference 15 describes a method that utilizes buffer states added to the initial set of states in order to differentially correct the reference trajectory into the full ephemeris. The differential corrector adjusts the position and velocity of each state, such that the discontinuities between integrated trajectory from one state to the next is less than  $10^{-6}$  km and  $10^{-9}$  km/s, respectively. The resulting trajectory is still discontinuous, however, the level of error is well below that of observed navigation of halo orbiters; hence the resulting trajectory can be considered operationally ballistic.<sup>16</sup> Once the differential corrector process is completed, the first and last revolution of the EML-1 orbit is pruned off, as described by Reference 15, resulting in four revolutions of a continuous orbit about EML-1.

### Trans-lunar Cruise

The trans-lunar cruise designed for this study is based on a possible crewed mission traversing EML-1 and EML-2. The trajectory involves a direct transfer to the Moon from a LEO parking orbit from a trans-lunar injection maneuver (TLI), followed by a powered lunar flyby, resulting in a direct transfer to an EML-2 halo orbit. This work only utilizes the first phase of the TLC from LEO to the powered lunar flyby. The full TLC to EML-2 is described since the trajectory is constrained to enter a 29.5 day (one synodic month) EML-2 halo orbit. This orbital period was chosen such that any crewed mission can launch a month late and have the same exact repeating geometry.

**Table 2. Initial LEO parking orbit conditions for TLI .**

Epoch	Orbital Parameters					
	Alt.	Ecc.	Inc.	RAAN	Arg. Per.	True Anom.
1/14/2020 00:00:00 ET	185 km	0.00	28.5 deg	223.144 deg	0 deg	-191.756 deg

The TLC begins from a LEO parking orbit with the orbital parameters given in Table 2. The transfer duration from LEO to the Moon is approximately 3.7 days. A delta-v of approximately 3.134 km/s in the along-track direction is used to insert into the TLC trajectory. A lunar flyby occurs at 1/17/2020 16:28:1.9163 ET. The lunar flyby occurs at an altitude of 100 km with a delta-v of approximately 213.56 m/s, performed at the periapse of the flyby. After the lunar flyby, the transfer to the EML-2 halo orbit is approximately 3.3 days. The crewed spacecraft reaches that halo insertion maneuver at 1/21/2020 00:00:00 ET with a delta-v of approximately 138.28 m/s.

## Ground Tracking Networks

During the Apollo era there existed 12 land-based and sea-based tracking stations that made up the Manned Space Flight Network. These stations were necessary in order to obtain reasonably accurate navigation estimates for early spaceflight. A subset of the Manned Space Flight Network was the DSN. The DSN is still operated today supporting various deep space missions that require accurate radiometric observations and communications. The DSN has three locations: Goldstone in California, Canberra in Australia, and Madrid in Spain. Another tracking network was defined during the Constellation program's 4B integrated design and analysis cycle (IDAC4B). This network is denoted as IDAC4B and utilizes the DSN and three additional tracking stations located at Santiago, Chile; Hartebeesthoek, South Africa; and Usuda, Japan. The location of these three tracking networks is shown in Figure 2. The IDAC4B stations are located in the opposite hemisphere of their corresponding DSN stations by a significant difference in latitude. This difference in latitude provides a significant geometrical advantage when using radiometric data yielding better navigation solutions using a smaller number of stations when compared to the Apollo tracking network.

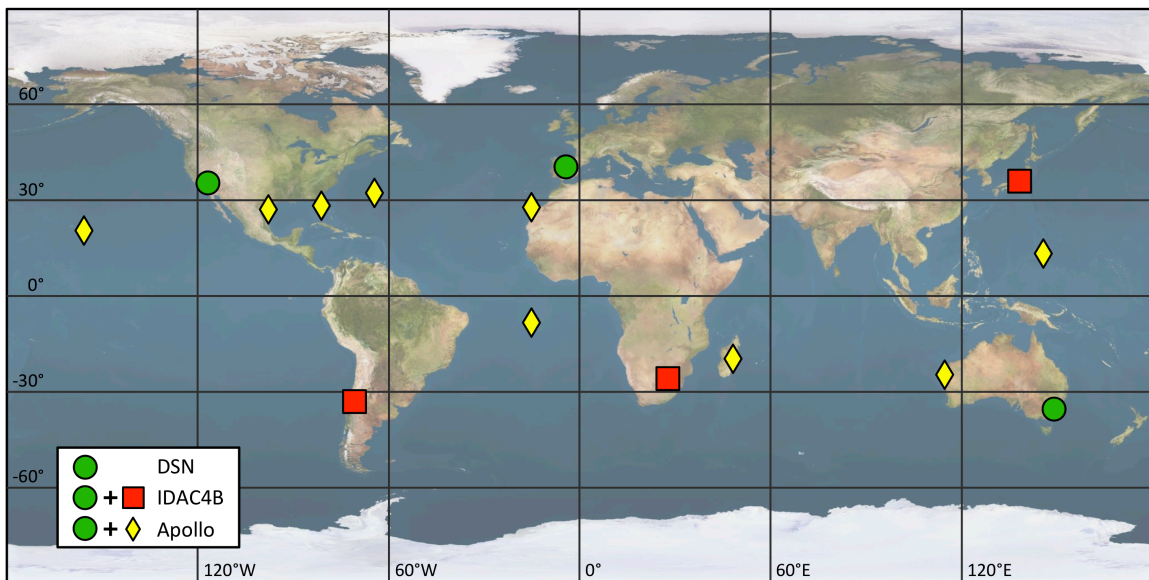


**Figure 2. Locations of the DSN, IDAC4B, and Apollo tracking networks. The DSN network is common for all of the tracking networks and is denoted by green circles; the IDAC4B network is denoted by red squares, and the Apollo stations are given by yellow diamonds.**

For this study, only the DSN and the IDAC4B tracking networks are used. It has previously been shown that the IDAC4B configuration is sufficient enough to obtain navigation uncertainties necessary for crewed spaceflight to the Moon.<sup>4,5</sup> The DSN stations continuously collect two-way range and range-rate measurements with a 10 deg elevation mask on a 100 s observation interval. The additional IDAC4B stations continuously collect three-way range and range-rate data with a 10 deg elevation mask on a 100 s observation interval. For this study, it is assumed that the crewed TLC spacecraft has access to the observations at all times for use in the onboard navigation.

## SPACECRAFT DYNAMICAS AND MODEL LINEARIZATION

The covariance analysis utilized in this work employs the propagation of the state and uncertainty along a defined reference trajectory followed by measurement processing to obtain an accurate estimate of the spacecraft's uncertainty. This method employs linearization of the states in order to propagate the uncertainty over time along the reference trajectory. The associated dynamical equations of motion and linearization are presented.

### Spacecraft Dynamics

This study is concerned with estimating the position and velocity of the LiAISON navigation satellite and the crewed spacecraft. Eq. 1 below gives the state vector that is being estimated

$$\mathbf{X} = [\mathbf{r}_1^T \quad \mathbf{v}_1^T \quad \mathbf{r}_2^T \quad \mathbf{v}_2^T \quad C_{R,1} \quad C_{R,2}]^T \quad (1)$$

where  $\mathbf{r}_i$  is the position (dimension 3) and  $\mathbf{v}_i$  is the velocity (dimension 3) for a given spacecraft  $i = 1, 2$ . The position and velocity vectors are both expressed in the Geocentric Celestial Reference Frame (GCRF). The remaining elements of the state vector are the SRP reflectivity coefficients, which will be defined later in this section.

The state vector  $\mathbf{X}$  is governed by a system of nonlinear first order differential equations. For this work, the time evolution of the position and velocity vectors of a spacecraft are given by

$$\begin{bmatrix} \dot{\mathbf{r}}_i \\ \dot{\mathbf{v}}_i \end{bmatrix} = \begin{bmatrix} \mathbf{v}_i \\ \mathbf{a}_{2-body}(t, \mathbf{r}_i) + \mathbf{a}_{nonspherical}(t, \mathbf{r}_i) + \mathbf{a}_{n-body}(\mathbf{r}_i, \mathbf{r}_{\oplus 3}) + \mathbf{a}_{SRP}(t, \mathbf{r}_i) \end{bmatrix} \quad (2)$$

where  $\mathbf{a}_{2-body}$  is the general two-body equation of motion,  $\mathbf{a}_{nonspherical}$  is the perturbing acceleration due to the nonspherical mass distribution of the central body, and  $\mathbf{a}_{n-body}$  are the perturbations due to a third body. In addition to these gravitational accelerations,  $\mathbf{a}_{SRP}$  is the perturbation due to solar radiation pressure. The gravitational potential including the two-body term is commonly given in terms of spherical harmonics as

$$U(x, y, z) = \frac{\mu}{r} \left[ 1 + \sum_{l=2}^{\infty} \sum_{m=0}^l \left( \frac{R}{r} \right)^l P_{l,m}(\sin \phi_{gc}) \{C_{l,m} \cos(m\lambda) + S_{l,m} \sin(m\lambda)\} \right]. \quad (3)$$

The normalized Cartesian spherical harmonic model is used in this work.<sup>17</sup> The acceleration vector from spherical harmonics is commonly given in a central body fixed based reference frame. For Earth, this is given as by International Terrestrial Reference Frame (ITRF) and for the Moon, it is given by Moon-Centered Moon-Fixed (MCMF) reference frame. For the conversion from ITRF to GCRF, the 1976 IAU Precession, 1980 IAU Nutation (no IERS corrections), Earth rotation parameters, and polar motion are used.<sup>18</sup> The Lunar Librations given by the JPL DE405 ephemeris are used for the conversion from MCMF to GCRF.<sup>19,20</sup>

The gravitational effects due to multiple bodies (n-body) are used as well as the two-body and nonspherical gravitational perturbations. This can include perturbations due to the Sun, Moon, or other planets. The acceleration  $\mathbf{a}_{n-body,k}$  due to the gravitational attraction of body  $k$  is given by

$$\mathbf{a}_{n-body,k} = -\mu_k \begin{bmatrix} \frac{\mathbf{r}_{k,sat}}{r_{k,sat}^3} + \frac{\mathbf{r}_{\oplus,k}}{r_{\oplus,k}^3} \end{bmatrix} \quad (4)$$

where  $\mu_k$  is the gravitational parameter of body  $k$ ,  $\mathbf{r}_{k,sat}$  is the position vector from body  $k$  to the satellite, and  $\mathbf{r}_{\oplus,k}$  is the position vector from the central body to the satellite  $k$ . The position of the celestial bodies can be obtained from the JPL DE405 ephemerides.<sup>19,20</sup>

A constant area and constant reflectance solar radiation pressure model is used. A shadow model is used that determines an approximate percentage of the Sun's face that is visible from the spacecraft location. The JPL DE405 ephemeris is used for the radii of the bodies used in the shadow model, and the solar radiation pressure is adjusted based on the distance from the sun.<sup>19,20</sup> The acceleration due to SRP is given by

$$\mathbf{a}_{SRP} = P_{SRP} C_R \frac{A_{\odot}}{m} \frac{\mathbf{r}_{\odot sat}}{|\mathbf{r}_{\odot sat}|} \quad (5)$$

where  $P_{SRP}$  is the solar radiation pressure of the Sun,  $C_R$  is the reflectivity coefficient of the spacecraft,  $A_{\odot}$  is the cross-sectional area,  $m$  is the mass of the spacecraft, and  $\mathbf{r}_{\odot sat}$  is the vector from the sun to the spacecraft.

### Dynamic Model Linearization

The full nonlinear dynamics need to be linearized in order to estimate the uncertainty of the spacecraft configuration. The linearization is performed using partial derivatives of the state with respect to an initial state from  $t_k$  to  $t_{k+1}$ . The two important linearized parameters are the state transition matrix

$$\Phi(t_{k+1}, t_k) = \frac{\partial \mathbf{X}(t_{k+1})}{\partial \mathbf{X}(t_k)} \quad (6)$$

and the process noise mapping matrix

$$\Gamma(t_{k+1}, t_k) = \frac{\partial \mathbf{X}(t_{k+1})}{\partial \mathbf{u}(t_k)} \quad (7)$$

where  $\mathbf{u}$  is the process noise. The state transition matrix is obtained by integrating

$$\dot{\Phi}(t, t_k) = A(t)\Phi(t, t_k) \quad (8)$$

subject to the initial conditions  $\Phi(t_k, t_k) = I$ . The Jacobian matrix  $A(t)$  is evaluated along the reference trajectory  $\mathbf{X}^*(t)$  and is given by

$$A(t) = \frac{\partial F(\mathbf{X}^*, t)}{\partial \mathbf{X}} \quad (9)$$

where  $F(\mathbf{X}^*, t)$  is the time derivative of the state vector.

## OBSERVATION MEASUREMENTS AND MODEL LINEARIZATION

In order to accurately estimate the uncertainty of the mission trajectories, it is necessary to describe the types of measurements that are collected. These measurements are used to determine the uncertainty in the satellite states and are generally nonlinear. The following sections give the full nonlinear measurement observations and their linearization for use in a covariance analysis.

### Measurement Models

In this study, a simplified measurement model is used that consists of an idealized range and range-rate measurement between the two satellites performing LiAISON and the ground network. Previous studies have shown that a complex model that solves for the time of flight is not significantly different for these studies when compared to the idealized range and range-rate measurement.<sup>21</sup> The idealized range between two satellites can be defined as

$$\rho = \sqrt{(\mathbf{r}_1 - \mathbf{r}_2) \cdot (\mathbf{r}_1 - \mathbf{r}_2)} + \rho_{bias} + \rho_{noise} \quad (10)$$

where  $\mathbf{r}_1$  and  $\mathbf{r}_2$  are the position vectors of the two satellites performing LiAISON. Similarly, the ground tracking range can be obtained by replacing the second satellite's position,  $\mathbf{r}_2$ , with the ground station position,  $\mathbf{r}_s$ . The error terms  $\rho_{bias}$  and  $\rho_{noise}$  are used to corrupt the idealized range.

The idealized range-rate between two satellites is expressed as

$$\dot{\rho} = \frac{\boldsymbol{\rho} \cdot \dot{\boldsymbol{\rho}}}{\rho} + \dot{\rho}_{noise} \quad (11)$$

where  $\boldsymbol{\rho} = \mathbf{r}_1 - \mathbf{r}_2$  is the position vector between the two satellites and  $\dot{\boldsymbol{\rho}} = \mathbf{v}_1 - \mathbf{v}_2$  is the relative velocity between the two satellites. Similar to the idealized range equation for ground tracking, the range-rate equation can be modified by assuming that the second satellite's velocity,  $\mathbf{v}_2$ , with the ground station velocity,  $\mathbf{v}_s$ . A noise term,  $\dot{\rho}_{noise}$ , is added to corrupt the idealized range-rate.

### Measurement Linearization

The nonlinear measurements need to be linearized in order to perform the uncertainty analysis for this study. The partial derivative of the measurements with respect to the state is necessary for the linearization. The generalized measurement equation is given by

$$\mathbf{Y} = \mathbf{h}(\mathbf{X}, \mathbf{u}) + \boldsymbol{\nu} \quad (12)$$

where  $\mathbf{h}$  is the nonlinear observation function and  $\boldsymbol{\nu}$  is the observation noise. For this study, the observation function is defined by

$$\mathbf{h}(\mathbf{X}, \mathbf{u}) = \left[ \rho_{LiAISON} \quad \dot{\rho}_{LiAISON} \quad \boldsymbol{\rho}_{ground}^T \quad \dot{\boldsymbol{\rho}}_{ground}^T \right]^T \quad (13)$$

The necessary observation linearization is given by

$$\tilde{H}_{\mathbf{X},k} = \frac{\partial \mathbf{h}}{\partial \mathbf{X}_k} \quad \text{and} \quad \tilde{H}_{\mathbf{u},k} = \frac{\partial \mathbf{h}}{\partial \mathbf{u}_k} \quad (14)$$

where  $k$  denotes a specific instance,  $t_k$ , that the linearization happens. Since the state is not dependent on the process noise  $\mathbf{u}$ , the second term in Eq. 14 is zero. The first term in Eq. 14 is non-zero and must be calculated analytically or numerically.

## NAVIGATION PERFORMANCE METHODS

### Crewed Vehicle Disturbance and Environment Modeling

This section describes nongravitational disturbances in the trajectory that are commonly caused by environmental venting and frequent attitude adjustments that are common to crewed vehicles. It is assumed that these disturbances are primarily due to: 1) wastewater dumps, 2) momentum desaturation maneuvers, 3) attitude control burns, 4) CO<sub>2</sub> venting, 5) thermal venting, and 6) water sublimation. These disturbances are increased during active crew cycles and are reduced during crew rest periods. These disturbances have been referred to as FLAK (Unfortunate Lack of Acceleration Knowledge).<sup>5</sup>

The term FLAK appeared during the Apollo program when it was determined that significant deviations in the trajectory occurred due to the activity of the crew and certain outgassing or maneuver events.<sup>1,2,5</sup> The current model used to estimate these disturbances is a simple state noise

compensation method.<sup>5</sup> Until a better model is developed, this simplistic FLAK model will be used to determine the necessary disturbance level. For the purpose of this work, a stochastic acceleration process is used to create a spherical position dispersion of 500 m (1- $\sigma$ ) every hour.

A discrete white noise process is used to drive the acceleration of the system that in turn induces errors in the position and velocity of the spacecraft. A linear discrete model for this system in one dimension is given by

$$\begin{bmatrix} x_{k+1} \\ v_{k+1} \\ a_{k+1} \end{bmatrix} = \begin{bmatrix} 1 & \Delta t & \Delta t^2/2 \\ 0 & 1 & \Delta t \\ 0 & 0 & 0 \end{bmatrix} \begin{bmatrix} x_k \\ v_k \\ a_k \end{bmatrix} + \begin{bmatrix} 0 \\ 0 \\ 1 \end{bmatrix} u_k \quad (15)$$

where  $\Delta t = t_{k+1} - t_k$  and  $u_k$  is the discrete Gaussian white noise process such that the statistics are  $E[u_k] = 0$  and  $E[u_i u_k] = q\delta_{i,k}$  where  $\delta_{i,k}$  is the Kronecker delta function. For the dynamic model and linearization used in this study, the state transition matrix and the process noise mapping matrix for one dimension of this system is defined as

$$\Phi(t_{k+1}, t_k) = \begin{bmatrix} 1 & \Delta t \\ 0 & 1 \end{bmatrix}, \quad \text{and} \quad \Gamma(t_{k+1}, t_k) = \begin{bmatrix} \frac{\Delta t^2}{2} \\ \Delta t \end{bmatrix} \quad (16)$$

This method can be assumed if the dynamics do not change significantly over a short duration of time. In order to determine the strength of the process noise  $q$  one needs to know the covariance  $\mathbf{P}_k$ . Reference 5 shows that if one assumes that the initial covariance  $\mathbf{P}_0$  is zero such that only the process noise used, the covariance  $\mathbf{P}_k$  can be calculated as

$$\mathbf{P}_k = q \begin{bmatrix} \frac{4n^3 - 3n^2 + 2n}{12} \Delta t^4 & \frac{n^2}{2} \Delta t^3 \\ \frac{n^2}{2} \Delta t^3 & n \Delta t^2 \end{bmatrix} \quad (17)$$

This derivation allows for more than one variation while achieving the same results such that the total propagation time  $T = n\Delta t$ . This shows that the same propagation time can result in different step sizes  $\Delta t$  and produce different values for  $\mathbf{P}_k$ . Thus, the process noise strength  $q$  must be computed in conjunction with the selection of a step size  $\Delta t$ .

If one assumes that  $\Delta t$  is small and thus  $n$  is very large, the covariance can be simplified and approximated by

$$\mathbf{P}_k \approx q \begin{bmatrix} \frac{n^3}{3} \Delta t^4 & \frac{n^2}{2} \Delta t^3 \\ \frac{n^2}{2} \Delta t^3 & n \Delta t^2 \end{bmatrix} \quad (18)$$

This result is the same as that found in Reference 5 and similar to that in Reference 22.

The only information concerning the strength of the process noise comes from the Apollo era. From the navigation solutions for Apollo missions, a trajectory deviation of several hundred meters was experienced over an hour in lunar orbit.<sup>1,2,5</sup> For this study, it is assumed that the uncertainty due to FLAK during TLC has a spherical position dispersion equivalent to 500 m (1- $\sigma$ ) over one hour. In order to determine the strength of the process noise in a single dimension, the position dispersion is equivalent to 288.6751 m. With a step size  $\Delta t$  of 100 s and a propagation time of 1 hour ( $n = 36$ ), the process noise strength is  $\sqrt{q} = 2.3148e-7$  km/s<sup>2</sup>. This process noise strength is used for active periods when the crew is awake and moving around. For quiet periods when the crew is asleep, the amount of FLAK is 10 times less ( $\sqrt{q} = 2.3148e-8$  km/s<sup>2</sup>).

## Cramér-Rao Covariance Study

In the realm of orbit determination, there are many sequential estimation algorithms used to estimate the state and uncertainty of a spacecraft. These applications generally require the estimation of unknown deterministic variables from a set of discrete nonlinear observations. Most practical estimation methods are not capable of estimating the optimal solution in such a way that it approaches the estimation error lower bound. The Cramér-Rao inequality is a very powerful tool that is used to estimate filter performance.<sup>23,24</sup> The Cramér-Rao lower bound (CRLB) can be calculated for any nonlinear system in which the truth trajectory is known and gives a limit on the best performance any nonlinear estimator can achieve. If  $\mathbf{P}_k$  is the estimation error covariance matrix corresponding to any unbiased estimator of a set of unknown states, and  $\mathbf{P}_k^*$  is the CRLB, then the inequality exists

$$\mathbf{P}_k \geq \mathbf{P}_k^* \equiv \mathbf{J}_k^{-1} \quad (19)$$

such that  $\mathbf{J}_k$  is the Fisher information matrix at time  $t_k$ . It has been shown that the extended Kalman filter covariance propagation equations linearized about the true trajectory correspond to the CRLB for a continuous-time nonlinear deterministic system with discrete nonlinear measurements.<sup>22</sup> Thus the recursive relationship for the Fisher information matrix is obtained by solving

$$\mathbf{J}_k = \left( \Phi(t_k, t_{k-1}) \mathbf{J}_{k-1}^{-1} \Phi(t_k, t_{k-1})^T \right)^{-1} + \tilde{H}_k^T \mathbf{R}_k^{-1} \tilde{H}_k \quad (20)$$

where  $\mathbf{R}_k$  is the observation weighting matrix. This recursion process is initialized by setting the initial Fisher information matrix  $\mathbf{J}_0 = \mathbf{P}_0^{-1}$ . This formulation works well for cases that do not have process noise. However, for the covariance study performed in this work, an additive noise is necessary. Thus Eq. 19 is modified to include process noise and takes the form

$$\begin{aligned} \mathbf{J}_k &= Q_{k-1}^{-1} + \tilde{H}_k^T \mathbf{R}_k^{-1} \tilde{H}_k \\ &\quad - Q_{k-1}^{-1} \Phi(t_k, t_{k-1}) \left( \mathbf{J}_{k-1} + \Phi(t_k, t_{k-1}) Q_{k-1}^{-1} \Phi(t_k, t_{k-1})^T \right)^{-1} \Phi(t_k, t_{k-1})^T Q_{k-1}^{-1} \end{aligned} \quad (21)$$

where  $Q$  is the process noise covariance. For this study,  $Q$  is computed such that

$$Q_k = \Gamma(t_k, t_{k-1}) q \Gamma(t_k, t_{k-1})^T \quad (22)$$

## TRANS-LUNAR CRUISE NAVIGATION PERFORMANCE

The results obtained in this section are for the TLC mission previously presented. Four tracking architecture types are analyzed: 1) DSN only, 2) IDAC4B only, 3) DSN and LiAISON, and 4) IDAC4B and LiAISON. Each simulation utilizes the same force models and measurement models. Both spacecraft are propagated using the GCRF coordinate system and are integrated using a point mass representation of Earth with third body perturbations due to the Sun and Moon using the JPL DE405 ephemeris. The TLC spacecraft uses a 20x20 spherical harmonic representation of the gravity field for both the Earth and Moon given by the GGM02C and LP150Q models respectively.<sup>25,26</sup> The  $C_R$  values for the TLC and EML-1 halo orbiter are 1.5 and 1.2 respectively. FLAK levels vary based on crew activity levels where there are 16 hours of active periods followed by 8 hours of quiet periods. The time evolution of the state dynamics is solved using the TurboProp orbit integration package for orbit propagation.<sup>27</sup> Initial state and measurement uncertainties are given in Table 3.

**Table 3. Navigation performance initial uncertainties.**

Estimation Parameters	<i>a priori</i> uncertainty (1- $\sigma$ )	Number of Parameters
TLC spacecraft position	1,000 m	3
TLC spacecraft velocity	500 m/s	3
EML-1 spacecraft position	100 m	3
EML-1 spacecraft velocity	1 m/s	3
SRP Coefficient	5%	2
Active FLAK	2.3148e-7 km/s <sup>2</sup>	—
Quiet FLAK	2.3148e-8 km/s <sup>2</sup>	—
LiAISON measurements		
range	1 m	—
range-rate	1 mm/s	—
Ground measurements		
range	2 m	—
range-rate	0.5 mm/s	—

### TLC with Standard FLAK Level

The best possible navigation uncertainties obtained in this study for a crewed vehicle using four different tracking architectures is shown in Figure 3. The results in Figure 3 show navigation uncertainties from just after TLI to just prior to the lunar flyby. Continuous range and range-rate measurements from each tracking source are taken every 100 s over the 3.7 day TLC.

The navigation results show that all navigation architectures approach steady state after 12 hours of tracking. DSN only tracking has the worst navigation uncertainty of all tracking architectures. When using the IDAC4B configuration only, navigation accuracies are reduced significant-

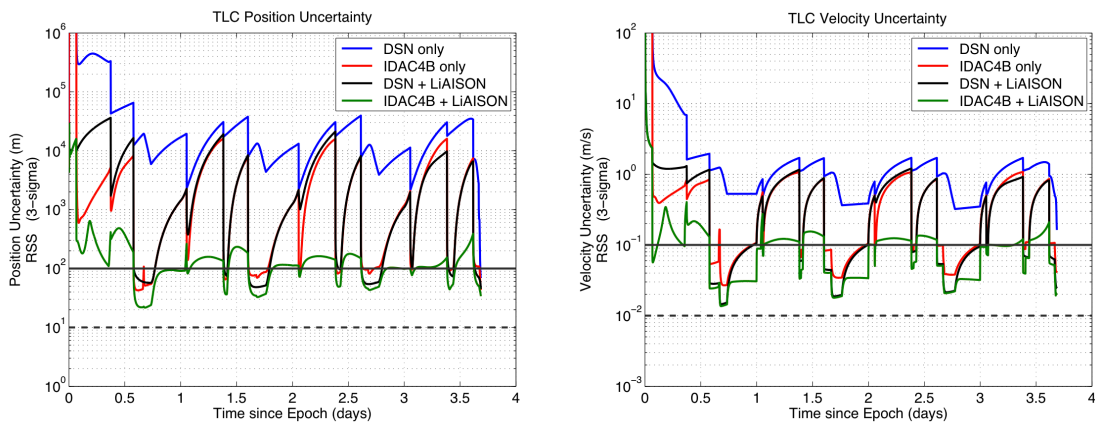


**Figure 3. Time history of the position and velocity RSS navigation uncertainty for four different tracking architectures. 1) DSN only (blue), 2) IDAC4B only (red), 3) DSN and LiAISON (black), and 4) IDAC4B and LiAISON (green). For position (velocity), the solid grey line represents 100 m (10 cm/s) uncertainty and the dashed grey line represents 10 m (1 mm/s) uncertainty.**

**Table 4. TLC navigation uncertainties.**

Architecture	3D-RMS Position Uncertainty (m)	3D-RMS Velocity Uncertainty (m/s)
DSN only	18,113.7	1.1028
IDAC4B only	5,467.3	0.5645
DSN + LiAISON	5,772.0	0.5713
IDAC4B + LiAISON	130.4	0.0996

ly from that of DSN only. When LiAISON measurements are introduced to the DSN only measurements, the navigation uncertainty is reduced to that of using only the IDAC4B configuration. The best possible navigation solution is achieved using the IDAC4B configuration with LiAISON measurements. The 3D-RMS position and velocity uncertainties are given in Table 4. The 3D-RMS values are calculated after steady state is reached at 12 hours until the lunar flyby occurs.

### Navigation Sensitivity to FLAK Level

The Apollo era acceleration uncertainties due to FLAK events may not correspond directly to future crewed missions to the Moon. This analysis varies the strength of the FLAK events to determine the navigation sensitivities due to the FLAK levels. Five different FLAK levels are chosen for this study. Each simulation uses the exact same observation measurements and uncertainties given in Table 3. FLAK levels are varied by 0.1, 0.5, 1, 2, and 5 times the acceleration uncertainty determined from the Apollo era assumption that the acceleration uncertainties due to FLAK events creates a 500 m dispersion in 1 hour.

The navigation sensitivities to the several different FLAK levels are shown in Figure 4 for both position and velocity. Similar to the previous analysis, the 3D-RMS values are calculated after steady state is reached at 12 hours until the lunar flyby occurs. FLAK levels are more sensitive to the DSN only, IDAC4B only, and DSN and LiAISON tracking architectures. The IDAC4B and LiAISON navigation architecture is the least sensitive to various FLAK levels. The navigation uncertainties are similar to the previous analysis such that DSN has the largest 3D-

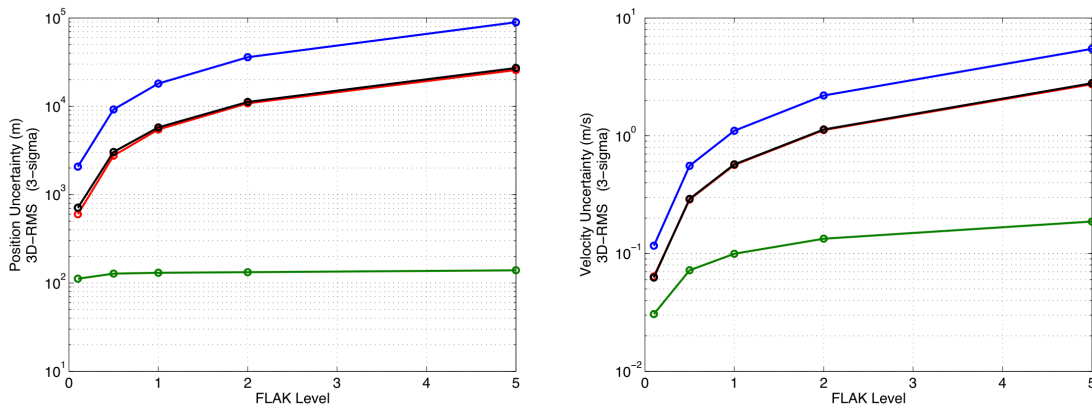


**Figure 4. Navigation sensitivities due to FLAK levels. 1) DSN only (blue), 2) IDAC4B only (red), 3) DSN and LiAISON (black), and 4) IDAC4B and LiAISON (green).**

RMS uncertainty while IDAC4B has the smallest uncertainty. IDAC4B only and DSN and LiAISON have nearly identical navigation uncertainties.

## CONCLUSION

The benefit of navigating a crewed vehicle between the Earth and the Moon using both ground tracking and satellite-to-satellite tracking was analyzed. Various navigation architectures, including ground-based and LiAISON supplemented configurations of a crewed mission to the Moon, were examined. A crewed trans-lunar cruise mission was designed with a navigation satellite located at EML-1. An acceleration uncertainty model based on historical Apollo data was derived to quantify the level of activity expected on a crewed vehicle. It was shown that a DSN only based tracking method has the worst position navigation uncertainty of about 18 km ( $3\text{-}\sigma$ ) for a standard FLAK level. The best navigation uncertainty was achieved using the six station IDAC4B configuration with a LiAISON based navigation satellite producing a position uncertainty of about 130 m ( $3\text{-}\sigma$ ). Navigation uncertainties were about the same for the IDAC4B only case and the DSN with LiAISON tracking case and resulted in position uncertainties of about 5.5 km ( $3\text{-}\sigma$ ). Various FLAK levels were also examined to determine the sensitivity of the navigation uncertainties due to unmodeled stochastic acceleration intensity. The least sensitive configuration to FLAK levels was determined to be the IDAC4B with LiAISON architecture. If the IDAC4B only tracking architecture can produce sufficient navigation uncertainty for crewed missions to the moon, then it could be substituted for three ground stations and one LiAISON satellite significantly reducing the cost of navigation for the crewed vehicle.

## ACKNOWLEDGMENTS

The authors would like to thank the JPL Center Innovation Fund (CIF) Program, sponsored by NASA Office of the Chief Technologist (OCT), which has supported this research.

The research presented in this paper has been partially carried out at the Jet Propulsion Laboratory, California Institute of Technology, under a contract with the National Aeronautics and Space Administration. Copyright 2012 California Institute of Technology. Government sponsorship acknowledged.

## REFERENCES

- <sup>1</sup> Wollenhaupt, W. R., "Apollo Orbit Determination and Navigation," *8<sup>th</sup> AIAA Aerospace Sciences Meeting*, New York, AIAA Paper 1970-27, Jan. 1970.
- <sup>2</sup> D'Souza, C., "Process Noise for Lunar Missions," *NASA Johnson Space Center*, 2006.
- <sup>3</sup> Getchius, J., Kubitschek, D. G., and Crain, T. P., "Orion Navigation Sensitivities to Ground Station Infrastructure for Lunar Missions," *AAS Guidance and Control Conference*, Univelt, San Diego, CA, 2008.
- <sup>4</sup> D'Souza, C., Getchius, J., Holt, G., and Moreau, M., "Lunar Navigation Architecture Design Considerations," *AAS Guidance and Control Conference*, Univelt, San Diego, CA, 2009.
- <sup>5</sup> Ely, T. A., Heyne, M., and Riedel, J. E., "Altair Navigation Performance During Translunar Cruise, Lunar Orbit, Descent, and Landing," *Journal of Spacecraft and Rockets*, Vol. 49, No. 2, March–April 2012.
- <sup>6</sup> Hill, K., Lo, M. W., and Born, G. H., "Linked, Autonomous, Interplanetary Satellite Orbit Navigation (LiAISON)," *AAS/AIAA Astrodynamics Specialist Conference*, No. AAS 05-399, AAS/AIAA, Lake Tahoe, CA, August 7–11, 2005.
- <sup>7</sup> Hill, K., Parker, J. S., Born, G. H., and Demandante, N., "A Lunar L2 Navigation, Communication, and Gravity Mission," *AIAA/AAS Astrodynamics Specialist Conference*, No. AIAA 2006-6662, AIAA/AAS, Keystone, Colorado, August 2006.
- <sup>8</sup> Hill, K. and Born, G. H., "Autonomous Interplanetary Orbit Determination Using Satellite-to-Satellite Tracking," *AIAA Journal of Guidance, Control, and Dynamics*, Vol. 30, No. 3, May–June 2007.

- <sup>9</sup> Hill, K., *Autonomous Navigation in Libration Point Orbits*, Ph.D. thesis, University of Colorado, Boulder, Colorado, 2007.
- <sup>10</sup> Parker, J. S., Anderson, R. L., Born, G. H., Fujimoto, K., Leonard, J. M., and McGranaghan, R. M., "Navigation between geosynchronous and lunar L1 orbiters," *AAS/AIAA Astrodynamics Specialist Conference*, No. AIAA-2012-4878, Minneapolis, MN, August 13 – 16, 2012.
- <sup>11</sup> Leonard, J. M., McGranaghan, R. M., Fujimoto, K., Born, G. H., Parker, J. S., and Anderson, R. L. "LiAISON-Supplemented Navigation For Geosynchronous and Lunar L1 Orbiters." *AAS/AIAA Astrodynamics Specialist Conference*, No. AIAA-2012-4664, Minneapolis, MN, August 13 – 16, 2012.
- <sup>12</sup> Angelopoulos, V., "The ARTEMIS mission." *Space science reviews*, Vol. 165, Issues 1 – 4, pp. 3-25, 2011.
- <sup>13</sup> Sweetser, T. H., Broschart, S. B., Angelopoulos, V., Whiffen, G. J., Folta, D. C., Chung, M. K., Hatch, S. J., and Woodard, M. A., "ARTEMIS Mission Design," *Space science reviews*, Vol. 165, Issues 1 – 4, pp. 27-57, 2011.
- <sup>14</sup> Richardson, D. L. and Cary, N. D., "A Uniformly Valid Solution for Motion of the Interior Libration Point for the Perturbed Elliptic-Restricted Problem," *AAS/AIAA Astrodynamics Specialist Conference*, No. AAS 75-021, AAS/AIAA, July 1975.
- <sup>15</sup> Parker, J. S., *Low-Energy Ballistic Lunar Transfers*, Ph.D. thesis, University of Colorado, Boulder, Colorado, 2007.
- <sup>16</sup> Folta, D., Woodard, M., and Cosgrove, D., "Stationkeeping of the First Earth-Moon Libration Orbiters: The ARTEMIS Mission," *Proceedings of the 2011 AAS/AIAA Astrodynamics Specialists Conference*, 2011.
- <sup>17</sup> Gottlieb, R. G., "Fast Gravity, Gravity Partial, Normalized Gravity, Gravity Gradient Torque and Magnetic Field: Derivation, Code and Data," *Tech. Rep. NASA Contractor Report 188243*, 1993.
- <sup>18</sup> Montenbruck, O. and Gill, E., *Satellite Orbits: Models, Methods and Applications*, Springer-Verlag, Netherlands, corrected 3rd printing 2005 ed., 2000.
- <sup>19</sup> Standish, E. M., "JPL planetary and lunar ephemerides, DE405/LE405," *Jet Propulsion Laboratory Interoffice Memorandum IOM 312F-98-048*, Aug. 26 1998.
- <sup>20</sup> Hoffman, D., *A Set of C Utility Programs for Processing JPL Ephemeris Data*, Johnson Space Center, 1998.
- <sup>21</sup> Fujimoto, K., Leonard, J. M., McGranaghan, R. M., Parker, J. S., Anderson, R. L., and Born, G. H., "Simulating the LiAISON Navigation Concept in a GEO + Earth-Moon Halo Constellation," *23rd International Symposium on Space Flight Dynamics*, Pasadena, CA, October 29 – November 2, 2012.
- <sup>22</sup> Crassidis, J. L., and Junkins, J. L., *Optimal Estimation of Dynamic Systems*, Chapman and Hall/CRC, Boca Raton, FL, 2004.
- <sup>23</sup> Taylor, J., "The Cramer-Rao estimation error lower bound computation for deterministic nonlinear systems," *IEEE Transactions on Automatic Control*, Vol. 24, No. 2, 1979, pp. 343{344.
- <sup>24</sup> Kerr, T. H., "Status of CR-like lower bounds for nonlinear filtering," *IEEE Transactions on Aerospace and Electronic Systems*, Vol. 25, No. 5, 1989, pp. 590-601.
- <sup>25</sup> Tapley, B., Ries, J., Bettadpur, S., Chambers, D., Cheng, M., Condi, F., Gunter, B., Kang, Z., Nagel, P., Pastor, R., Pekker, T., Poole, S., and Wang, F., "GGM02 - An Improved Earth Gravity Field Model from GRACE," *Journal of Geodesy*, Vol. 79, No. 8, 2005, pp. 467-478.
- <sup>26</sup> Konopliv, A., S. W. Asmar, E. Carranza, W. L. Sjogren, and D. Yuan, "Recent Gravity Models as a Result of the Lunar Prospector Mission," *Icarus*, Volume 150, 2001, pp. 1–18.
- <sup>27</sup> Hill, K. and Jones, B. A., *TurboProp Version 4.0*, Colorado Center for Astrodynamics Research, May 2009.